UC Irvine

UC Irvine Previously Published Works

Title

Two-photon microscopy reveals early rod photoreceptor cell damage in light-exposed mutant mice.

Permalink

https://escholarship.org/uc/item/0qj446pk

Journal

Proceedings of the National Academy of Sciences of USA, 111(14)

Authors

Maeda, Akiko
Palczewska, Grazyna
Golczak, Marcin
et al.

Publication Date

2014-04-08

DOI

10.1073/pnas.1317986111

Peer reviewed

eScholarship.org Powered by the California Digital Library
University of California

Two-photon microscopy reveals early rod photoreceptor cell damage in light-exposed mutant mice

Akiko Maeda[a,b,1,2], Grazyna Palczewska[c,1,2], Marcin Golczak[a], Hideo Kohno[a], Zhiqian Dong[c], Tadao Maeda[a,b], and Krzysztof Palczewski[a,2]

Departments of [a]Pharmacology and [b]Ophthalmology and Visual Sciences, Case Western Reserve University, Cleveland, OH 44106; and [c]Polgenix Inc., Cleveland, OH 44106

Edited by Constance L. Cepko, Howard Hughes Medical Institute, Harvard Medical School, Boston, MA, and approved February 25, 2014 (received for review September 23, 2013)

Atrophic age-related and juvenile macular degeneration are especially devastating due to lack of an effective cure. Two retinal cell types, photoreceptor cells and the adjacent retinal pigmented epithelium (RPE), reportedly display the earliest pathological changes. *Abca4*$^{-/-}$*Rdh8*$^{-/-}$ mice, which mimic many features of human retinal degeneration, allowed us to determine the sequence of light-induced events leading to retinal degeneration. Using two-photon microscopy with 3D reconstruction methodology, we observed an initial strong retinoid-derived fluorescence and expansion of *Abca4*$^{-/-}$*Rdh8*$^{-/-}$ mouse rod cell outer segments accompanied by macrophage infiltration after brief exposure of the retina to bright light. Additionally, light-dependent fluorescent compounds produced in rod outer segments were not transferred to the RPE of mice genetically defective in RPE phagocytosis. Collectively, these findings suggest that for light-induced retinopathies in mice, rod photoreceptors are the primary site of toxic retinoid accumulation and degeneration, followed by secondary changes in the RPE.

In recent years, dramatic progress has been made in discovering genetic and environmental factors contributing to retinal diseases. Imaging modalities such as scanning laser ophthalmoscopy (SLO) and optical coherence tomography along with classic histological methods and functional techniques, such as electroretinography (ERG) and electrophysiological recordings, have facilitated characterization of retinal defects (1–3). Concurrently, molecular understanding of the chemistry and biology of vision has paved the way for the first successful treatment of inherited retinal diseases, such as Leber congenital amaurosis (4–6) or the advanced exudative form of age-related macular degeneration (AMD) (7, 8). However, identifying the cell type where the pathology originates and understanding the underlying pathological mechanisms have remained a challenge, impeding progress toward development of therapies effective against several common retinal diseases.

A tight interconnection between the neuronal retina and retinal pigmented epithelium (RPE) is essential for flow of nutrients, retinoids, and metabolic products (9, 10). Detachment of the retina from the RPE leads to rapid retinal atrophy in vivo. Because of this functional interrelationship between the RPE and photoreceptors and lack of well-developed experimental methodologies, it is difficult to assess which cells are initially affected by pathology in retinal diseases such as Stargardt disease or AMD. Even with suitable rodent models of blinding diseases, access to individual cell types in their native settings remains a challenge.

To identify the sequence of degenerative processes in the retina initiated by brief intense light exposure, we first selected a mouse model that exhibits many features associated with human Stargardt disease and AMD—namely, *Abca4*$^{-/-}$*Rdh8*$^{-/-}$ mice (11, 12). These genetically modified mice lack both the ATP-binding cassette transporter 4 (ABCA4) and the *all-trans*-retinol (ROL) dehydrogenase enzyme (RDH8). Both proteins are involved in the retinoid cycle, a metabolic sequence of chemical transformations needed to maintain continuous regeneration of the visual chromophore, 11–*cis*–retinal (11cRAL) from *all-trans*-retinal (atRAL), and both are also required for efficient clearance of atRAL upon its liberation from activated rhodopsin (13–17). Impaired clearance of atRAL is detrimental to retinal cells due to the high toxicity of this reactive aldehyde to all cell types (18). Clearance of atRAL is achieved by ABCA4, which transports atRAL from the disk lumen to the cytoplasmic space of photoreceptor outer segments (19) where RDHs, including RDH8, then reduce atRAL to ROL (11, 20). Defective ABCA4 function has been associated with both Stargardt disease (21) and AMD (22). Other than atRAL itself, condensation products of atRAL, including diretinoid-pyridinium-ethanolamine (A2E) formed in the RPE can also cause retinal degeneration (23). Formation of A2E is normally a relatively slow process requiring several biochemical reactions in photoreceptor and RPE cells (24, 25). A2E overaccumulation is observed in the RPE of individuals with Stargardt disease and is a risk factor for AMD. This by-product can thus serve as a marker of atRAL-associated changes and/or

Significance

Identifying the sequence of events underlying light-induced pathology is important for understanding the mechanisms leading to retinal degeneration, and consequently for development of therapies against retinal diseases. In this study, we characterized the early phase of retinal degeneration using two-photon microscopy, mass spectroscopy, and genetically modified mice. We identified rod photoreceptors as the initial locus of degeneration. Primary changes included retinoid-dependent formation of fluorescent metabolic by-products within rod photoreceptor cells and a nearly three-fold expansion/swelling of rod outer segments. These changes were followed by secondary infiltration of microglia/macrophages to clear photoreceptor cell debris. Finally, we provide evidence that phagocytosis-mediated transfer of rod-derived toxic compounds to the retinal pigmented epithelium is required to elicit damage to that cell layer.

Author contributions: A.M., G.P., M.G., H.K., T.M., and K.P. designed research; A.M., G.P., M.G., H.K., Z.D., and T.M. performed research; H.K. contributed new reagents/analytic tools; A.M., G.P., Z.D., and K.P. analyzed data; and A.M., G.P., M.G., T.M., and K.P. wrote the paper.

The authors declare no conflict of interest.

This article is a PNAS Direct Submission.

[1]A.M. and G.P. contributed equally to this work.

[2]To whom correspondence may be addressed. E-mail: kxp65@case.edu, aam19@case.edu, or gmp26@case.edu.

This article contains supporting information online at www.pnas.org/lookup/suppl/doi:10.1073/pnas.1317986111/-/DCSupplemental.

direct toxicity to the retina (1, 26–28). Identification of the primary cause of retinal degeneration, whether it is atRAL or its condensation products, as well as determination of which cell types are initially affected comprise two particularly intriguing questions that need answers to guide the development of optimal therapeutic interventions.

Brief exposure of *Abca4*$^{-/-}$*Rdh8*$^{-/-}$ mice to intense light results in acute retinal degeneration, which allows investigators to follow the precise sequence of degenerative events at both a cellular and molecular level (18, 29). Notably, such retinal degeneration can be prevented by inhibition of atRAL production with retinylamine, a retinoid cycle inhibitor (30), or by sequestration of atRAL by producing Schiff-base adducts of atRAL with drugs containing a primary amine group (12, 29). The *Abca4*$^{-/-}$*Rdh8*$^{-/-}$ mouse also exhibits slowly progressive retinal degeneration under normal lighting conditions with a phenotype similar to AMD that responds to the above treatments (29). Downstream consequences of atRAL-induced cellular toxicity have also been studied, and pharmacologic inhibition of certain downstream targets can prevent atRAL-induced cell death (31).

To monitor the flow of retinoids in the retinas of *Abca4*$^{-/-}$*Rdh8*$^{-/-}$ mice after bright light exposure, we developed fluorescent imaging techniques with 3D reconstruction that take advantage of the fluorescent properties of certain isoprenoids and their condensation products. Noninvasive, high-resolution imaging of the retina was achieved by using two-photon microscopy (TPM), which offers real time, high-resolution images of endogenous fluorescent molecules in living tissues (32, 33). These methods, along with supplementary histological approaches, were used here to gain insights into the initiation of photoreceptor cell/RPE pathologies in *Abca4*$^{-/-}$*Rdh8*$^{-/-}$ mice after bright light exposure.

Now, we provide evidence indicating that light-induced production of atRAL in *Abca4*$^{-/-}$*Rdh8*$^{-/-}$ mice causes RPE-independent degeneration of photoreceptor cells. Moreover, we show that active phagocytosis of affected photoreceptor cells by the RPE is required for the development of pathological changes in the RPE. Taken together, these results support a model whereby the primary site of pathology is photoreceptor cells, with RPE degeneration developing as a consequence of phagocytosis of excess atRAL condensation products accumulated primarily in rod outer segments (ROS) after light exposure.

Results

TPM noninvasively images autofluorescence (AF) signals from retinosomes containing *all-trans* retinyl esters (RE) and atRAL condensation products in RPE cells (32–38). As previously reported, retinosomes and other AF signals were observed in RPE cells of albino 4-wk-old *Abca4*$^{-/-}$*Rdh8*$^{-/-}$ mice (32) (Fig. 1*A*). Additionally, we observed AF signals from photoreceptor outer segments (OS) (Fig. 1*A*), indicating that these AF products could be formed in the OS and then possibly be transferred to the RPE through phagocytosis. Thus, we aimed to identify the origin and site of formation of these AF products through extensive kinetic analyses of light-induced pathology in *Abca4*$^{-/-}$*Rdh8*$^{-/-}$ mice by several complementary techniques, including genetic manipulations, TPM, ERGs, and liquid chromatography/mass spectrometry (LC/MS).

Characterization of Retinal AF and Function in *Abca4*$^{-/-}$*Rdh8*$^{-/-}$ Mice After Bright Light Exposure. To monitor temporal changes in AF properties of OS and RPE, we examined albino 4-wk-old *Abca4*$^{-/-}$*Rdh8*$^{-/-}$ mice at different time intervals after a 60-min exposure to light at 10,000 lx. Using TPM of intact mouse eyes, we observed an abundance of small AF spots in the OS at days 1 and 3 after light exposure (Fig. 1*A*, *Upper*). Moreover, ~10× larger AF granules were detected in the OS layer at day 3 after light exposure as well. At day 11 after light exposure, small rounded AF spots, most likely representing OS, were no longer visible. Furthermore, some infiltrating cells with more elongated shapes, likely representing microglia/macrophages, were noted in the subretinal space (Fig. 1*A*, *Upper*). In parallel with the OS changes, we also noted that the intensity of AF particles located in the RPE near cell boundaries increased at days 1 and 3 after light exposure (Fig. 1*A*, *Lower*). These AF particles were clearly visible with 730 nm, but not with 850 nm, light (Fig. 1*A* and Fig. S1*A*). At day 11 after exposure, signals from these AF particles

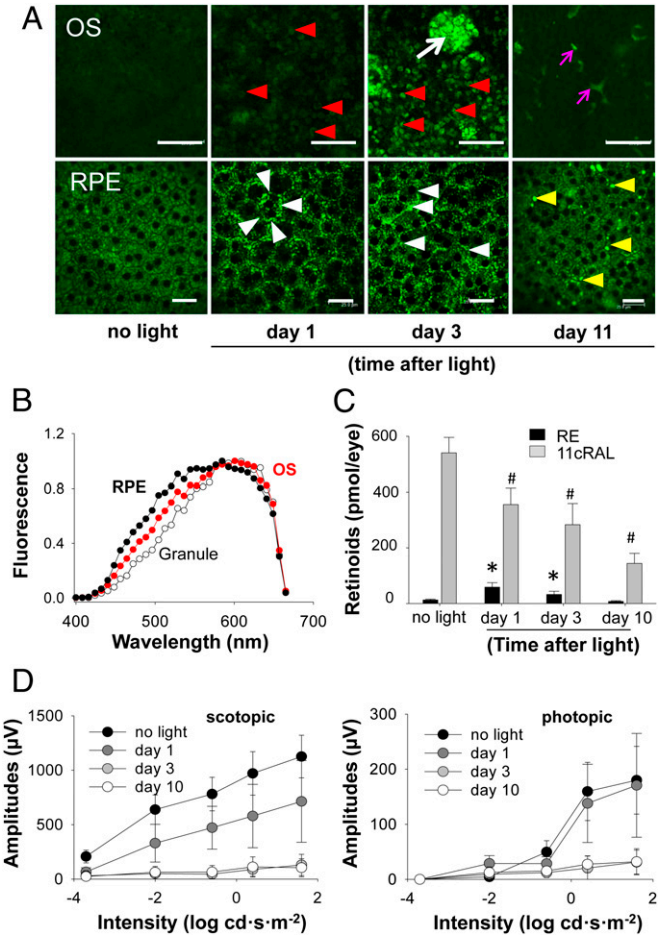

Fig. 1. Time course of changes in the retina of *Abca4*$^{-/-}$*Rdh8*$^{-/-}$ (Dko) mice after bright light exposure. Dko mice with an albino background at 4 wk of age were exposed to 10,000 lx light for 60 min, and then kept in the dark until evaluation. (*A*) TPM images obtained with 730 nm excitation before and at days 1, 3, and 11 after light exposure. Photoreceptor outer segment layer images are shown (*Upper*). Faint at day 1 and more easily visible at day 3 after light exposure, round AF spots (red arrowheads) were observed. Large AF granules (white arrow) were visualized at day 3 after light. At day 11 after illumination, AF-elongated shapes (magenta arrows) were seen. (Scale bars: 25 μm.) RPE images displaying characteristic double-nuclei structures (*Lower*). AF particles located close to the RPE cell–cell junctions at days 1 and 3 after exposure are indicated with white arrowheads. AF particles, observed at day 11 after light exposure, are designated with yellow arrowheads. (*B*) At day 3 after light exposure, AF TPM emission spectra were obtained from the RPE layer, the ROS round spots, and large granules. (*C*) Amounts of retinyl esters (RE) and 11cRAL in the eye were quantified by HPLC on indicated days after light exposure. Error bars indicate SD of the means ($n = 5$). $^{*}P < 0.05$ in RE and $^{\#}P < 0.05$ in 11cRAL vs. values obtained in no-light-exposed mice. (*D*) Retinal function evaluated by ERG recordings decreased significantly at day 1 from rod ($P < 0.05$ at all stimulus intensities by one-way ANOVA) but not cone photoreceptors ($P > 0.5$ by one-way ANOVA at a stimulus intensity greater than −2 log cd·s·m^{-2}) and then disappeared entirely from both types of photoreceptors at days 3 and 10 after light exposure. Error bars indicate SD of the means ($n = 3$).

had decreased, but different types of AF signals from larger particles distributed randomly within RPE had appeared (Fig. 1*A*, *Lower*). These new AF particles were also clearly visible with 850 nm excitation at day 11 after light exposure (Fig. S1*A*). We have used the ratio between fluorescence recorded with excitation light at 850 nm and 730 nm to quantify changes in the fluorescent properties of these two AF signals over time (Fig. S1*B*).

To further characterize the origin of observed AF signals in OS and RPE, we analyzed the emission spectrum of AF by TPM of intact eyes of albino 4-wk-old *Abca4*$^{-/-}$*Rdh8*$^{-/-}$ mice at day 3 after 60-min light exposure at 10,000 lx. AF spectra from the small fluorescent spots in OS and RPE showed similar patterns (Fig. 1*B*), except the OS spectra revealed a greater impact of fluorophores emitting at longer wavelengths with a broad maximum at 600 nm. AF emission spectra from the larger granules attributed to infiltrating microglia/macrophages more closely resembled those from the OS than from the RPE, suggesting that these granules were loaded with AF debris from dying photoreceptor cells.

Because the amount of 11cRAL in the retina correlates well with the numbers of photoreceptors and can be used to quantify the severity of retinal degeneration (12), we used HPLC to analyze retinoids in the eye. Here we found that 11cRAL content in *Abca4*$^{-/-}$*Rdh8*$^{-/-}$ mouse eyes had decreased by 37.9% at day 1 after light exposure and by 73.4% at day 10 (Fig. 1*C*). In contrast, RE content increased at days 1 and 3 and then decreased at day 10 after light illumination. This change in RE content also correlated well with the increase in AF elicited from particles observed in the RPE at days 1 and 3 after light exposure, and likely was due to retinosome expansion (33). The prolonged elevated presence of RE could be a result of compromised function of the retinoid cycle caused by the early demise of photoreceptors as indicated by the appearance of fluorescent products in the rod outer segments and further implied by the reduced quantity of 11cRAL.

Retinal function assessed by ERG recordings showed decreased responses (12) (Fig. 1*D*). These ERG results indicate that substantial rod cell demise had occurred without detectible loss in cone function by day 1 after bright light exposure. Moreover, ERG signals were not detected in either rods or cones at day 3 and 10 after such exposure. These findings in *Abca4*$^{-/-}$*Rdh8*$^{-/-}$ mice are consistent with progressive degeneration of both types of photoreceptor cells with greater resistance exhibited by cones to light-induced damage (39).

We further assessed the changes in WT mice. Littermate control WT mice of *Abca4*$^{-/-}$*Rdh8*$^{-/-}$ mice were not light insensitive and did not show light-induced retinal degeneration under the same light exposure conditions as studies with *Abca4*$^{-/-}$*Rdh8*$^{-/-}$ mice. As expected, no abnormal AF signals were detected by TPM imaging (Fig. S2*A*). Next, BALB/c mice were evaluated. Mice were exposed to 20,000 lx for 120 min to cause light-induced retinal degeneration. Damaged OS and RPE displayed AF abnormalities similar to those observed in *Abca4*$^{-/-}$*Rdh8*$^{-/-}$ mice (Fig. S2*B*). These observations indicate that AF changes in OS and RPE are closely associated with retinal damage.

Three-Dimensional TPM Images Reveal the Shape and Distribution of AF Signals in the Retina. AF signals from 4-wk-old *Abca4*$^{-/-}$*Rdh8*$^{-/-}$ mouse eyes (Fig. 2, *Top*) unexposed to light were uniformly distributed throughout the RPE cell layer as previously reported (32). However, here we also detected small uniformly distributed AF spots that appeared more like the tips of columns in our 3D reconstruction, extending from 8 μm under the RPE into the retinal space. Before light exposure, these AF spots were small and faint (Fig. 2, *Top*). At day 3 after light exposure (Fig. 2, *Middle*), irregular, larger, and brighter AF doughnut-like spots, most likely due to dying photoreceptors, were seen extending from 8 μm under the RPE into the retinal space. At about the same depth, we also detected AF granules with diameters over

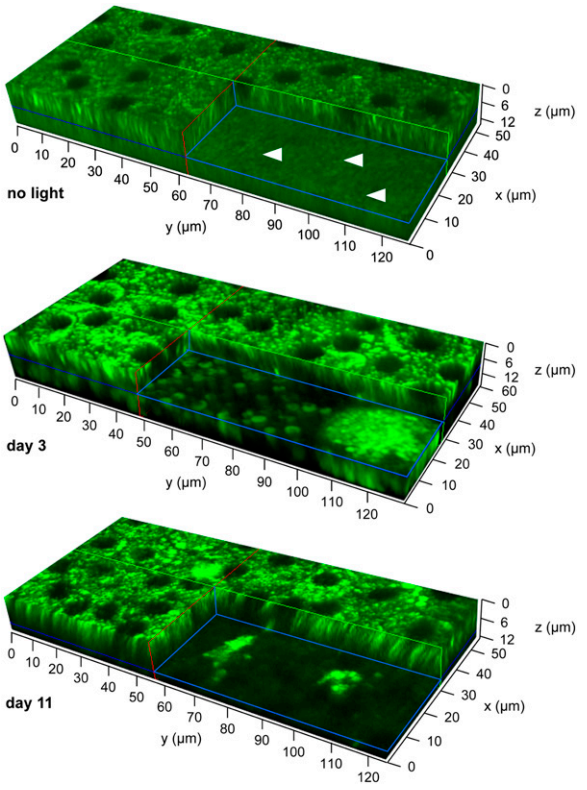

Fig. 2. Temporal changes in AF particles after light exposure. TPM images of intact Dko mouse eyes after 10,000 lx light exposure for 60 min. In each 3D TPM section, the RPE is at the top as indicated by 0 μm on the *z* axis and the ROS are underneath. Without light exposure, only small weak AF spots were detected in the plane located 8 μm below the RPE layer, as indicated by white arrowheads (*Top*). However, both round doughnut-shaped AF spots and large AF granules were located ∼8 μm beneath the RPE at day 3 after light exposure (*Middle*). At day 11 after light exposure, round doughnut-shaped AF spots were no longer present, but predominant larger AF shapes were extending to deeper level (∼12 μm) beneath the RPE (*Bottom*).

25 μm, likely representing microglia/macrophages. At day 11 after light exposure (Fig. 2, *Bottom*), doughnut-like spots were no longer present, and the larger AF granules with varying round to elongated shapes were extended deeper in to the subretinal space.

Subretinal Translocation of Microglia in the Retinas of *Abca4*$^{-/-}$*Rdh8*$^{-/-}$ Mice After Light Exposure. Damaged cells were largely cleared by day 11 (Fig. 1*A*). Thus, aided by a few initial clues, we explored possible mechanism(s) for this clearance. First was the supposition that the ∼25-μm diameter AF cells observed in the OS layer shown in Fig. 1*A* could represent infiltrating microglia/macrophages (40, 41). Translocation of microglia/macrophages into the subretinal space is one of the features of retinal inflammation found in degenerating retinas (42, 43). A second concern was that even though retinal infiltrating cells had been imaged by SLO as AF granules in *Abca4*$^{-/-}$*Rdh8*$^{-/-}$ mice after light illumination (41, 42), neither their fluorescence spectra nor their z location within the retina were known. Here we found increased numbers of SLO AF granules at day 3 that peaked at day 7 after light exposure [Fig. 3*A*, *Left* (images) and *Right* (quantification)]. To definitively identify the type of cell(s) infiltrating the RPE/retina junction, we then investigated microglial translocation in *Cx3cr1*$^{Gfp/\Delta}$*Abca4*$^{-/-}$*Rdh8*$^{-/-}$ mice with microglia expressing GFP (44). Fluorescent imaging of their retinal sections after 10,000 lx light exposure for 60 min revealed microglia with round instead of ramified shapes translocated from the inner retina into the

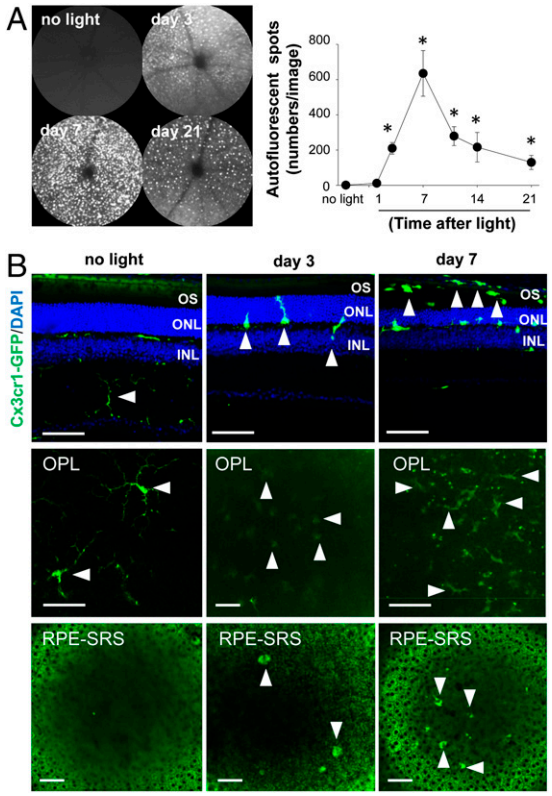

Fig. 3. Numbers of AF microglia/macrophages in Dko mice after light exposure. (*A*) Dko mice with a pigmented background at 4 wk of age were exposed to 10,000 lx light for 30 min and then kept in the dark until evaluation. Representative SLO images after light exposure are presented at days 3, 7, and 21 after light exposure (*Left*). Numbers of AF granules identified by SLO after light exposure were counted on the indicated day (*Right*). Bars indicate SD ($n = 5$). *$P < 0.05$ vs. no light exposure. (*B*) *Cx3cr1*$^{gfp/\Delta}$*Abca4*$^{-/-}$*Rdh8*$^{-/-}$ mice with an albino background at 4 wk of age were exposed to 10,000 lx light for 60 min. Microglial translocation was examined by fluorescent imaging (*Top*) and by TPM imaging at indicated depths of the retina (*Middle* and *Bottom*). Microglial cells (arrowheads) in these mice exhibited GFP expression because of their *Cx3cr1*$^{gfp/\Delta}$ genotype. DAPI was used to stain nuclei. INL, inner nuclear layer; ONL, outer nuclear layer; OPL, outer plexiform layer; SRS, subretinal space. (Scale bars: 50 μm.)

subretinal space (Fig. 3*B*, *Top*). These changes were also detected in intact mouse eyes by TPM imaging (Fig. 3*B*, *Middle* and *Bottom*). Before light exposure, only ramified GFP-expressing microglial cells were detected in the outer plexiform layer (Fig. 3*B*, *Middle Left*). At days 3 and 7, post-light-exposure changes observed by TPM in intact eyes included increased numbers of microglia with more-rounded shapes at the same locations (Fig. 3*B*, *Middle Center* and *Middle Right*). Round-shaped microglia cells also were more frequently detected in the subretinal space at days 3 and 7 after light exposure. Notably, infiltrating microglia in the subretinal space displayed a stronger AF intensity, probably due to their phagocytosis of OS debris (Fig. 3*B*, *Bottom Center* and *Bottom Right*).

Light Exposure Alters Retinoid Metabolite Profiles of the Retina. Fluorophores responsible for AF in the retina could be an indicator of global changes in the metabolic profile of this tissue. To evaluate and quantify these changes as well as determine whether they depend on a functional retinoid cycle, we used both genetically altered (*Lrat*$^{-/-}$) and pharmacologically treated (retinylamine) mice with metabolic profiles that were compared with light-exposed and dark-adapted *Abca4*$^{-/-}$*Rdh8*$^{-/-}$ mice by using a LC/MS approach. Mouse retinas were isolated either on day 3 after light exposure (10,000 lx for 30 min) or from animals kept in the dark as controls. Metabolites were extracted with acetonitrile and subjected to MS analysis (Fig. 4). XCMS software was used to compare the data from individual samples that were grouped in analytically replicated datasets (45). Approximately 1,700 individual ions in the mass range of 200 to 2,000 *m/z* were aligned in these mouse retinal extract replicates. Almost 8% of all signals detected in these datasets demonstrated significant changes in their relative intensities (defined as a ≥1.5-fold change with $P \leq 0.01$). Notably, a given molecule could be represented by several different signals corresponding to differing isotopic distributions or nonspecific adducts. Nevertheless, these comparative data revealed that the most profound differences in ion composition between light-exposed and control retinal samples were detected during an HPLC retention period of 5–15 min and these included dramatic increases in several ion intensities in the mass range of *m/z* 220 to *m/z* 750 (Fig. 4*A*, *Upper* and Fig. 4*B*, *Top*). Additional ions with elevated intensities in light-exposed samples were observed at 22 min of elution. To investigate the origin of these light-induced alterations, we first analyzed the metabolic profile of retinal samples isolated from light-exposed lecithin:retinol acyltransferase (LRAT)-deficient mice that cannot produce visual chromophore (46). Here among

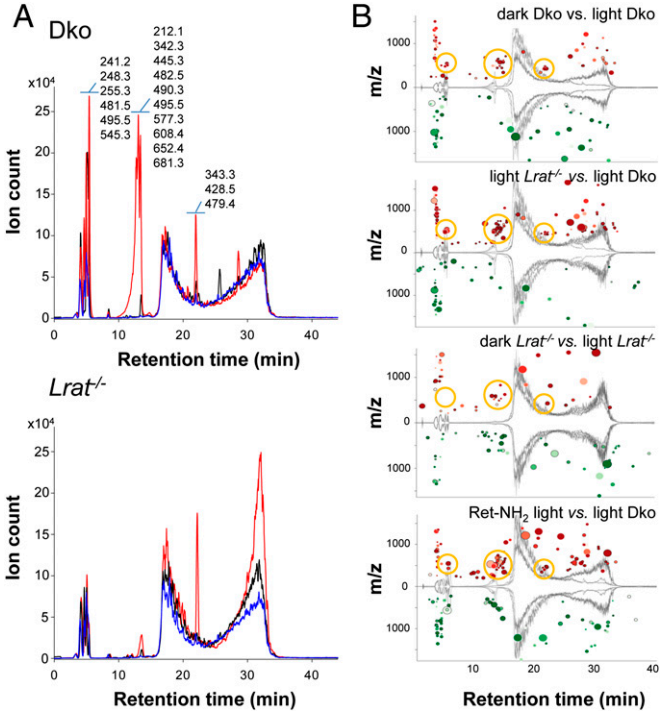

Fig. 4. Light-induced differences in metabolic profiles of mouse retina. Analysis of light-induced differences in metabolic profiles of mouse retina. (*A*) (*Upper*) Base peak ion chromatograms for retinal extracts obtained from dark-adapted (black trace) and, at day 3 after light exposure (red trace), Dko mice. The blue line corresponds to samples obtained from retinylamine (Ret–NH_2) treated animals. The same color scheme was used for chromatograms obtained from *Lrat*$^{-/-}$ mice (*Lower*; blue line indicates Ret–NH_2-treated Dko retinas). (*B*) The most characteristic ions overrepresented in light-exposed samples are shown. Differences between analyzed samples are represented in differential feature plots with the minimal fold-change threshold set at 1.5 and *P* value threshold at <0.01. In this representation, the most dominant increase in ion intensities found in light-exposed retinas vs. reference samples are shown in red, whereas suppressed ions are marked in green. The size of each circle represents the log-fold change. The shade of the color corresponds to the *P* value (the darker the color, the lower the *P* value). The most characteristic common clusters of ions for light-exposed samples are circled in yellow (see *Results*).

1,850 aligned individual ions, 174 showed significant signal changes. Although, there were spurious peaks most likely arising from differences in genetic background, the same set of ions eluted between 5 and 15 min that were identified previously in the light *Abca4*$^{-/-}$*Rdh8*$^{-/-}$ (Dko) vs. dark Dko plot were clearly visible (Fig. 4*A*, *Lower*). However, importantly, unlike the peak with a retention time around 22 min, these ion signals did not appear in the differential plot of light-exposed vs. dark-adapted *Lrat*$^{-/-}$ retinas (Fig. 4*B*), suggesting that they originated as a result of visual pigment activation. As an alternative to the above genetic approach, regeneration of visual chromophore in the eye was also markedly reduced by pretreatment of *Abca4*$^{-/-}$*Rdh8*$^{-/-}$ mice with an inhibitor of the retinoid cycle, retinylamine (30), several hours before light exposure. Again, as noted with LRAT-deficient samples, the most significant difference in the ion profiles occurred between 5 and 15 min of elution and involved an identical set of *m*/*z* values (Fig. 4*B*, *Bottom*). In summary, light-induced alteration of the metabolic profile in the retina was dependent not only upon activation of functional visual pigment but also on its continuous effective regeneration with chromophore via the retinoid cycle. Thus, the observed effects can be linked to an excess of atRAL generated in photoreceptor cells. Although indirect, these data also support the idea that elevated atRAL levels play a critical role in retinal degeneration.

Changes in Photoreceptor OS at Day 1 After Light Exposure. To obtain more detailed information about changes in the OS, we used TPM to image retinal tissues lacking the RPE ex vivo. Here, albino 4-wk-old *Abca4*$^{-/-}$*Rdh8*$^{-/-}$ mice were exposed to light at 10,000 lx for 60 min and their retinas were harvested and stripped of the RPE at day 1 after light exposure. Such processed retinas were immediately analyzed by TPM. Photoreceptor OS in unexposed retinas lacking the RPE were uniformly distributed, showing a tight, regular arrangement (Fig. 5*A*, *Upper*). However, the OS of retinas at day 1 after light exposure displayed doughnut-like shapes, enlarged diameters, and shortened lengths (Fig. 5*A*, *Lower* and Fig. 5 *B* and *C*). Measurements of these OS diameters were 3.67 ± 0.73 μm in light-exposed mice and 1.43 ± 0.19 μm in unexposed control animals.

Photoreceptor Cell Apoptosis Is Caused by atRAL in Neural Retinal Tissue Culture. The primary cause of acute retinal degeneration after bright light exposure in *Abca4*$^{-/-}$*Rdh8*$^{-/-}$ mice is the delayed clearance of atRAL from photoreceptors (18). Moreover, light-induced retinal degeneration in *Abca4*$^{-/-}$*Rdh8*$^{-/-}$ mice can be prevented by pharmacological interventions such as the retinoid cycle inhibitor with a primary amino group, retinylamine (12, 30), and the NAPDH oxidase inhibitor, apocynin (31, 47–49) (Fig. S3). Thus, to examine whether retinal tissue lacking RPE cells can display degenerative changes similar to those observed in in vivo, we performed ex vivo culture experiments with retinal explants coincubated with atRAL. Neural retinas were dissected from eyes of 4-wk-old WT mice, and incubated with 30 μM of atRAL in the presence of control vehicle, 30 μM of retinylamine or 300 μM of apocynin for 6 h at 37 °C. Coincubation of atRAL with control vehicle resulted in marked retinal degeneration (Fig. 6*A*), and massive photoreceptor apoptosis was observed upon TUNEL staining (Fig. 6*B*). However, coincubation of atRAL with either retinylamine or apocynin prevented photoreceptor apoptosis in these retinal explant tissue cultures. Cell death rates were calculated by measuring lactate dehydrogenase released into tissue culture supernatants from dying cells. These calculated rates also indicated that atRAL-induced cell death in the neural retina was largely prevented by coincubation with retinylamine and apocynin (Fig. 6*C*), similar to results obtained in *Abca4*$^{-/-}$*Rdh8*$^{-/-}$ mouse retina (Fig. S4).

Last, retinas of WT mice were incubated with 30 μM of atRAL for 24 h followed by TPM analysis. Notably, a spectrum similar to

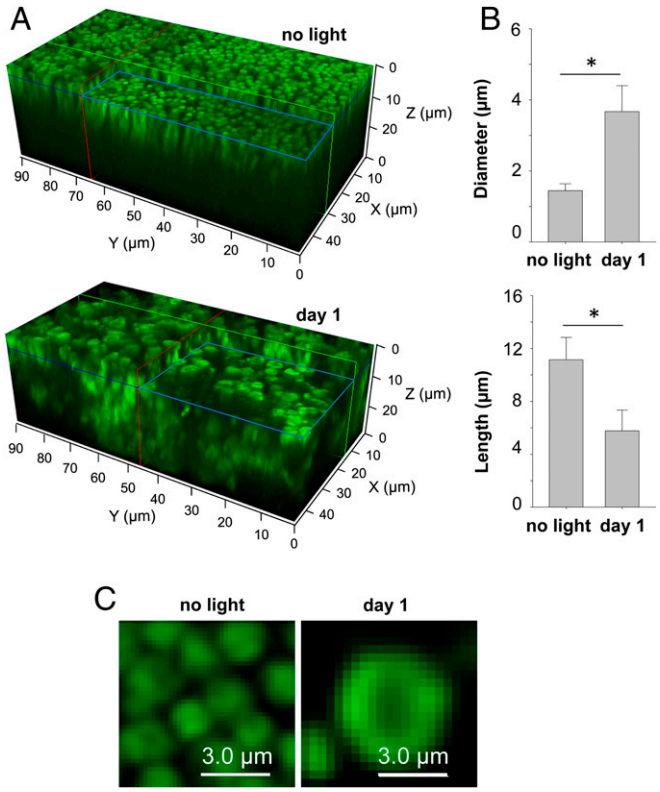

Fig. 5. Dko mice exhibit enlargement of photoreceptor cell outer segments at day 1 after light exposure. Dko mice with an albino background at 4 wk of age were exposed to 10,000 lx light for 60 min and then kept in dark until evaluation. TPM imaging was carried out at day 1 after light exposure immediately after retinas were removed from their eyecups and stripped of the RPE. Retinas for TPM were placed in 3-cm dishes with DMEM. (*A*) Outer segment tips are at the top, as indicated by 0 μm on the *z* axis. (*Upper*) A 3D TPM section shows regularly arranged photoreceptors in the retina from a mouse unexposed to light. (*Lower*) A 3D TPM section reveals ROS with enlarged diameters and darker centers in a mouse retina at day 1 after light exposure. (*B*) Diameters and lengths of ROS from mice unexposed to light and at day 1 after light exposure are presented. *$P < 0.05$ vs. no-light-exposed mice. (*C*) Magnified views of the ROS XY sections from retinas in *A* are shown.

that of OS after light exposure in vivo (Fig. 1*B*) was obtained from the OS of retinal tissues incubated with atRAL (Fig. 6*D*, *Left*). Interestingly, the OS in retinal tissues incubated with or without atRAL showed enlarged diameters (Fig. 6*D*, *Right*), suggesting that retinal tissue culture conditions can induce OS damage as well. These results with the neural retinal tissue culture indicate that retinal degeneration is initiated by photoreceptor cell death independent of the RPE in *Abca4*$^{-/-}$*Rdh8*$^{-/-}$ mice, and thus pathological changes in RPE cells appear to be secondary events. Furthermore, the same experiments also establish that TPM can reveal initial degenerative changes that occur in ROS.

RPE and ROS Changes in *Abca4*$^{-/-}$*Rdh8*$^{-/-}$ Mice After Light Exposure. After bright light exposure, acute changes in OS over time were followed by changes in the RPE as shown by histological and immunocytochemical analyses. We studied the integrity of the RPE layer stained with an antibody against zonula occludentes (ZO-1), a resident protein of epithelial and endothelial cell membranes (50) associated with tight junctions. Two weeks after bright light exposure (10,000 lx for 60 min), changes in RPE layer were observed in 6-wk-old *Abca4*$^{-/-}$*Rdh8*$^{-/-}$ mice. Some RPE cells lost their expression of ZO-1 as indicated with the yellow arrowheads in Fig. S5*A*. After light exposure, vertical cross-sections

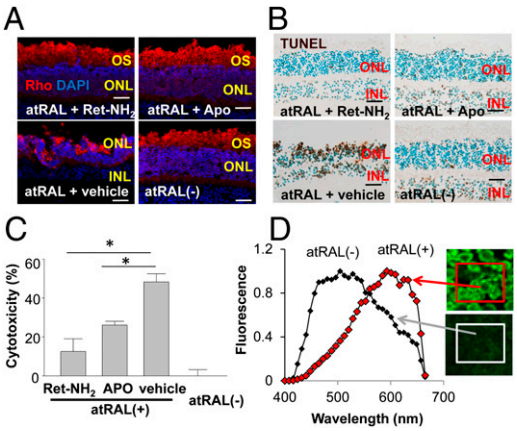

Fig. 6. Retinal degeneration is induced by atRAL in ex vivo retinal cultures. Retinas were removed from the eyecups of 4-wk-old C57BL/6J mice and cultured for 16 h at 37 °C. Then retinas were incubated further with/without 30 μM of atRAL in the presence/absence of experimental drugs for 6 h at 37 °C. Vehicle (DMSO), retinylamine (Ret–NH_2) at 30 μM, or apocynin (Apo) at 300 μM was applied, together with atRAL. (*A*) Retinal morphology was examined after incubation with atRAL and with and without drugs. Cryosections were prepared and photoreceptor outer segments were stained with anti-rhodopsin (Rho) (red) antibody, and nuclear staining was achieved with DAPI (blue). The ONL was markedly disrupted in atRAL/vehicle-treated mice in contrast to either Ret–NH_2- or apocynin-treated mice. (Scale bars: 20 μm.) (*B*) TUNEL staining (brown) was performed with the ApoTag Peroxidase in Situ Apoptosis Detection Kit. Counter nuclear staining was accomplished with methyl green (light blue). As in *A*, cotreatment with either Ret–NH_2 or APO protected the ONL and INL against atRAL-induced damage. (Scale bars: 20 μm.) (*C*) An LDH assay was carried out with the LDH activity assay kit (BioVision) to calculate cell death rates in retinal culture supernatants. atRAL caused retinal cell death which was reduced by coincubation with either retinylamine or apocynin. Bars indicate SD ($n = 3$). *$P <$ 0.05. (*D*) Retinas were removed from eyecups of 4-wk-old C57BL/6J mice and cultured with or without 30 μM of atRAL for 24 h at 37 °C. After incubation, retinas were washed twice with PBS and then examined by TPM. Spectra from photoreceptor outer segments are shown (*Left*) along with representative magnified images (*Right*). Spectra from retinas cultured with atRAL featured a broad maximum absorption at ∼600 nm.

(Fig. S5 *B* and *C*) of the retina and horizontal sections (Fig. S5*D*) at the RPE level started to show changes, including a reduced size of cells and nuclei and a darker staining of cytosol, indicating cellular damage (Fig. S5*E*). Because RPE cells are postmitotic, they expand to fill space caused by RPE cellular defects (51). Shortened and disrupted OS and chromatin condensation in photoreceptor nuclei were observed at day 3 after light exposure (Fig. S6*A*). EM analyses revealed that photoreceptor cell debris included fragmented OS and IS between the RPE and outer nuclear layers of *Abca4*$^{-/-}$*Rdh8*$^{-/-}$ mice at day 3 after light exposure (Fig. S6*B*). Fragmented photoreceptor debris and RPE cells also elicited AF signals from cryosections of retinas at day 3 after light exposure (Fig. S6*C*). Together these data suggest that light exposure results in a deterioration of RPE cells following changes in ROS.

AF Changes in *Mertk*$^{-/-}$*Abca4*$^{-/-}$*Rdh8*$^{-/-}$ Mice. Finally, we used another genetic approach to probe light-induced degenerative changes in mouse retina. Phagocytosis of OS by the RPE is dramatically attenuated in *Mertk*$^{-/-}$ mice (52–54). To determine whether retinal degeneration is initiated primarily by photoreceptor cell death in *Abca4*$^{-/-}$*Rdh8*$^{-/-}$ mice, we investigated AF in retinas of *Mertk*$^{-/-}$*Abca4*$^{-/-}$*Rdh8*$^{-/-}$ mice. *Mertk*$^{-/-}$*Abca4*$^{-/-}$*Rdh8*$^{-/-}$ mice at the age of 3 wk were exposed to light at 10,000 lx for 60 min, and TPM analysis was performed at days 3 and 7 after exposure. TPM imaging of AF in the OS and RPE of intact eyes in *Mertk*$^{-/-}$*Abca4*$^{-/-}$*Rdh8*$^{-/-}$ mice did not reveal any increase in the quantity of AF particles in the RPE compared with those seen in *Mertk*$^{-/-}$*Abca4*$^{-/-}$*Rdh8*$^{-/-}$ mice that were not exposed to light (Fig. 7 and Fig. S7*A*). However, disrupted OS structures were noted even in mice unexposed to light (Fig. S7*B*), providing an early sign indicative of retinal degeneration. Retinal histology then was examined in *Mertk*$^{-/-}$*Abca4*$^{-/-}$*Rdh8*$^{-/-}$ mice. Subretinal accumulation of photoreceptor debris was seen in plastic-embedded histological sections (Fig. S7*C*). Although light exposure caused photoreceptor damage and morphological sections manifested as decreased numbers of photoreceptors (Fig. S7*C*), accumulation of photoreceptor cell debris in the subretinal space was evident by both TPM and histological analyses even at day 7 after light exposure, despite the presence of microglia/macrophages (Fig. S8). Together, these observations indicate that AF particles that appear in the RPE at days 7 and 11 after light exposure in *Abca4*$^{-/-}$*Rdh8*$^{-/-}$ mice could represent phagocytized materials from dead photoreceptor cells.

Discussion

Here, we identified the sequence of changes in the retina that occurs as a consequence of exposure to brief strong illumination. *Abca4*$^{-/-}$*Rdh8*$^{-/-}$ mice were used as an animal model that mimics fundamental changes in the retina relevant to human Stargardt disease and AMD. We provide clear evidence that the primary changes in the retina include retinoid-dependent formation of fluorescent metabolic by-products within rod photoreceptor cells, a nearly three-fold expansion/swelling of the ROS, and secondary infiltration of microglia/macrophages to clear photoreceptor cell debris. Finally, evidence is provided that phagocytosis-mediated transfer of retinoid adducts to the RPE is required to elicit damage to that cell layer.

Retinal inflammation is closely associated with the pathogeneses of human retinal diseases, including retinitis pigmentosa, Stargardt disease, and AMD (43, 55). Moreover, infiltrating macrophages are thought to participate in the inflammation associated with retinal degeneration (56–58). Retinal macrophages

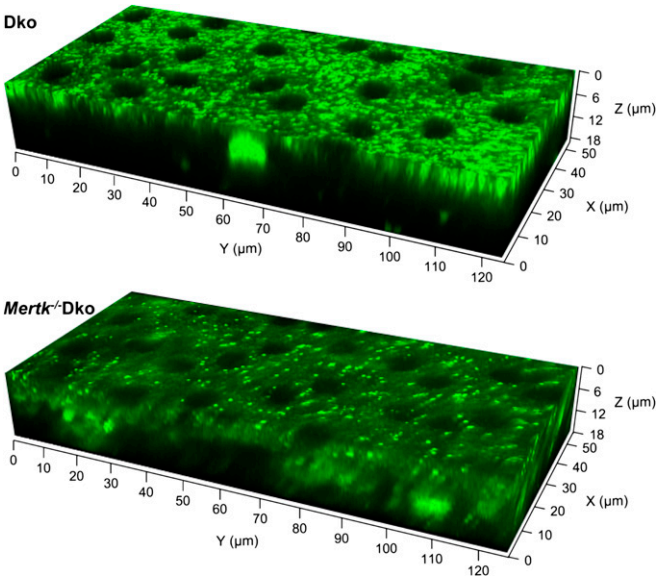

Fig. 7. Differences in RPE AF between Dko and *Mertk*$^{-/-}$Dko mice at day 7 after light exposure. *Mertk*$^{-/-}$*Abca4*$^{-/-}$*Rdh8*$^{-/-}$ (*Mertk*$^{-/-}$Dko) and Dko mice with an albino background at 3 wk of age were exposed to 10,000 lx light for 60 min, and 3D TPM images were obtained at day 7 after light exposure. Three-dimensional images of a Dko and a *Mertk*$^{-/-}$Dko mouse retina are shown in *Upper* and *Lower*, respectively. RPE in Dko exhibited an increased accumulation of AF spots, whereas no such changes were noted in *Mertk*$^{-/-}$Dko mice.

are subdivided into tissue-resident microglia of the inner retina and peripheral macrophages that migrate to this site from retinal blood vessels (40). Recent studies suggest a pathogenic role for subretinal macrophages (42, 59), even though they contribute to the clearance of photoreceptor cell debris. In this work, subretinal microglia/macrophages elicited an AF signal with a similar spectrum in both ROS and RPE cells, also suggesting subretinal microglia/macrophage involvement in clearing of ROS debris. This AF feature enabled the application of TPM and 3D reconstruction used in this study to monitor the sequence of events in the retinas of mice after bright light exposure (Figs. 1, 2, 5, and 7 and Figs. S1, S2, and S7).

Although the exact chemical composition of fluorescent products observed in the eye after light exposure was not identified, we provide evidence that such products were formed in a retinoid-dependent manner based on genetic considerations in conjunction with MS analyses (Fig. 4). Retinoids are highly reactive compounds prone to oxidation, isomerization, fragmentation, and condensation both with themselves and other membrane and protein components (60, 61). atRAL along with its derivative products likely are the initiators of photoreceptor cell pathology for several reasons: (*i*) phototransduction is the only light-sensitive pathway in ROS and this process involves the conversion of retinoids and generation of atRAL (62, 63); (*ii*) such light-induced degeneration can be prevented by pretreatment with retinoid cycle inhibitors (Fig. S3); and (*iii*) both retinoids and their condensation products are known to produce cellular toxicity and death (12, 18, 31, 64, 65). Retinal pathology could also result from mitochondrial dysfunction, because lipophilic unsaturated compounds such as retinoids can also act as electron acceptors that compromise ATP production (66–69).

For years it has been known that the lengths of ROS are reduced when animals are exposed to light for prolonged periods (70–73), but the molecular mechanism(s) remain obscure (74). Here, we observed that even though the length of ROS was reduced upon exposure to bright light, the volume of ROS expanded over approximately threefold. Advanced noninvasive TPM methods revealed swelling of ROS with increased AF disk diameters as early as 1 d after light exposure. Moreover, these changes in photoreceptor geometry were paralleled by differences in metabolic profiles of these retinas as determined by LC/MS at day 3 after exposure to light. Importantly, the imaging experiments were performed in a native setting with undisturbed intact eyes, which avoided potential artifacts arising from required tissue-processing. Although ROS sizes are known to be determined by rhodopsin content (75–78), these light-induced changes were too rapid for de novo protein biosynthesis to account for them. Additionally, it had been shown that rhodopsin mislocalized significantly to rod inner segments only at 48 h after light-induced damage (74). Thus, an osmotically driven influx of water after light exposure appears the most likely explanation for swelling of the ROS. Specifically without light exposure, the volume of the fluorescent portion of outer segments would be

$$\pi r^2 \times h = 3.14 \times 0.715^2 \times 11.12 = 17.8 \ \mu m^2,$$

whereas at day 1 after light exposure, the fluorescent portion of ROS was dramatically increased to

$$V = \pi r^2 \times h = 3.14 \times 1.835^2 \times 5.73 = 60.6 \ \mu m^2.$$

Thus, this expansion was not due to simple shortening of the compromised ROS. A plausible sequence of events could involve lower production of ATP, resulting in increased ion retention (79) and osmotic pressure that in turn cause bursting of ROS followed by photoreceptor death. Previously it was reported that ATP insufficiency is correlated with the failure of the plasma membrane to maintain Ca^{2+} pump function with subsequent overaccumulation of Ca^{2+} (80, 81). Also it is known that photoreceptor cells die rapidly when retinas are incubated in medium deficient in glucose or other metabolites that fuel ATP biosynthesis (82).

In recent years, we identified several approaches that reduce the damaging effects of intense light exposure. First, we found that retinylamine, by inhibiting the retinoid cycle, had the beneficial side effect of decreasing atRAL levels and toxicity (18). That work led to the discovery that other primary amines could exert the same protective effect on the retina (12). Then we discovered that a number of enzymes and receptors, including a subset of other G protein-coupled receptors, could also be targeted for potential therapy (31).

However, the above findings did not answer the critical question of whether the neuronal retina or the RPE was the primary target of therapy. Ex vivo retinal tissue cultures have enabled isolated studies of retinal function, including the recording of single cell responses (83). Notably, retinal explants can also be used to monitor changes in the retina independent of the RPE (84, 85). Here, we used ex vivo retinal tissue cultures to examine whether photoreceptor cells could degenerate without any contribution from RPE cells and found that coincubation of retinal tissues with atRAL caused photoreceptor cell apoptosis. Moreover, this apoptosis was prevented by coculture of retinal tissue with either retinylamine or apocynin, which also conferred protection against light-induced retinal degeneration in vivo. These experiments clearly identify photoreceptor cells as the primary targets for light-induced retinal degeneration and primary amine-mediated protection, but they do not exclude the RPE as a possible secondary target.

Detrimental actions of A2E accumulated in the RPE have been reported, including photosensitization (86, 87) and complement activation (88). However, it is not known whether these are a primary cause of retinal degenerative changes. Precursors of A2E formed in photoreceptor cell OS eventually reach RPE cells because the ends of the continuously renewed OS adjoining the RPE are removed by RPE cell phagocytosis (10). To examine the contribution of atRAL condensation products to retinal degeneration in *Abca4*$^{-/-}$*Rdh8*$^{-/-}$ mice, we generated *Mertk*$^{-/-}$*Abca4*$^{-/-}$*Rdh8*$^{-/-}$ mice that cannot carry out RPE phagocytosis (53). These mice still exhibited photoreceptor cell death without RPE phagocytosis after bright light exposure. Moreover, the RPE of these mice failed to display any AF changes, clearly indicating that A2E is not the primary initiator of light-induced retinal degeneration in this mouse model. However, *Mertk*-deficient mice did reveal infiltration of microglia/macrophages into the subretinal space (42, 52), indicating that these cells likely contribute to the clearance of photoreceptor cell debris.

In conclusion, we used a sophisticated imaging technique (TPM along with 3D reconstruction) supported by other classical methods to study retinal structure/function, which revealed a sequence of light-induced changes in *Abca4*$^{-/-}$*Rdh8*$^{-/-}$ and *Mertk*$^{-/-}$*Abca4*$^{-/-}$*Rdh8*$^{-/-}$ mice. These changes involved the formation of fluorescent retinoid by-products along with swelling of ROS and death of photoreceptor cells. The demise of photoreceptor cells was followed by secondary minor changes in the RPE involving altered cell shapes and sizes with accumulation of fluorescent products. These findings are likely to be relevant to many retinal degenerative processes that lead to devastating loss of vision, including human Stargardt disease and AMD.

Materials and Methods

Animals. *Abca4*$^{-/-}$*Rdh8*$^{-/-}$ mice were generated as described previously (29), and all mice were genotyped by well-established methods with the following primers for: *Abca4* WT, 5′-GCCCAGTGGTCGATCTGTCTAGC–3′ and 5′-CGGACACAAAGGCCGCTAGGACCACG-3′; *Abca4* mutant, 5′- CCACAGCACACATCAGCATTTCTCC-3′ and 5′-TGCGAGGCCAGAGGCCACTTGTGTAGC-3′; *Rdh8*

WT, 5′-CTTCAAAGTCAGTGGTGACTGGG-3′ and 5′-GCTATCCAGCTGCGACA-ATTC-3′; and *Rdh8* mutant, 5′-TCCGCCTTGGAAACCTGAGCCAGAAG-3′ and 5′- TGCGAGGCCAGAGGCCACTTGTGTAGC-3′ (12, 32, 42). *Mertk*$^{-/-}$ and *Cx3cr1*$^{gfp/\Delta}$ mice were purchased from The Jackson Laboratory. *Mertk*$^{-/-}$*Abca4*$^{-/-}$*Rdh8*$^{-/-}$ and *Cx3cr1*$^{gfp/\Delta}$*Abca4*$^{-/-}$*Rdh8*$^{-/-}$ mice were generated by cross-breeding and then genotyped. Genotyping for *Mertk*$^{-/-}$ or *Cx3cr1*$^{gfp/\Delta}$ mice was performed with primers for: *Mertk* WT, 5′-GCTTTAGCCTCCCCAGTAGC-3′ and 5′–GGTCA-CATGCAAAGCAAATG–3′; *Mertk* mutant, 5′–CGTGGAGAAGGTAGTCGTACATCT-3′ and 5′-TTTGCCAAGTTCTAATTCCATC-3′; *Cx3cr1* WT, 5′-TCCACGTTCGGTCT-GGTGGG-3′ and 5′-GGTTCCTAGTGGAGCTAGGG-3′; and *Cx3cr1–GFP* mutant, 5′-GATCACTCTCGGCATGGACG-3′ and 5′-GGTTCCTAGTGGAGCTAGGG-3′ according to the protocol from The Jackson Laboratory. *Lrat*$^{-/-}$ mice were bred and genotyped as detailed previously (46, 89) with primers for *Lrat* WT, 5′-AAGTGCTGGGCATGGTGACTTGTG-3′ and 5′-TCCAGTTCCAGACTCTTTCCACCCAC-3′ and for *Lrat* mutant, 5′-TGCGAGGCCAGAGGCCACTTGTGTAGC-3′ and 5′-TCCAGTTCCAGACTCTTTCCACCCAC-3′. Only *Rd8* mutation free mice with the Leu variation at amino acid 450 of RPE65 were used. Either pigmented C57BL/6J or albino C57BL/6J (C57BL/6J–*Tyr*$^{c-2J}$/J) mice from The Jackson Laboratory and their littermates were used as WT controls. BALB/c mice were obtained from The Jackson Laboratory. All mice were housed in the animal facility at the School of Medicine, Case Western Reserve University, where they were maintained on a normal mouse chow diet either under complete darkness or in a 12-h light (~10 lx)/12-h dark cyclic environment. Manipulations with retinas and retinoid extractions were done in the dark under dim red light transmitted through a Kodak No. 1 safelight filter (transmittance >560 nm). All animal procedures and experiments were approved by the Case Western Reserve University Animal Care Committees and conformed to both the recommendations of the American Veterinary Medical Association Panel on Euthanasia and the Association of Research for Vision and Ophthalmology.

Chemicals. AtRAL, ROL, and apocynin were purchased from Sigma-Aldrich; a mixture of 0.5% tropicamide and 0.5% phenylephrine hydrochloride (Midorin-P) was obtained from Santen Pharmaceutical Co. Ltd.; xylazine/AnaSed was from LLOYD, Inc.; and ketamine/Ketaset CIII was from Fort Dodge Animal Health. Retinylamine was synthesized from retinal as previously detailed (30, 34).

Induction of Retinal Light Damage. Mice were dark-adapted for 12–48 h before exposure to bright light. Acute retinal damage was induced by exposing animals to 10,000 lx of diffuse white fluorescent light for either 30 min (pigmented mice) or 60 min (albino mice). For BALB/c mice, 20,000 lx for 120 min were used to induce retinal damage with EcoSmart 42 W, color temperature 2,700 K, 2,800 lumens, model 28942BD bulbs (Commercial Electric). The bulb irradiance spectrum was recorded with a calibrated spectroradiometer Specbos 1211 UV (JETI Technische Instrumente GmbH). The resulting bulb spectrum had maxima at 620, 550, 450, 405, and 340 nm, with normalized amplitudes of 1, 0.7, 0.49, 0.28, and 0.13, respectively. Before each exposure, mouse pupils were dilated with a mixture of 0.5% tropicamide and 0.5% phenylephrine hydrochloride. After light exposure, animals were kept in the dark until evaluation.

TPM Imaging. TMP images were obtained with a Leica TCS SP5 confocal MP system equipped with an upright DM6000 CFS stand. A tunable laser Vision S (Coherent) delivered 75-fs laser light pulses at an 80-MHz pulse repetition frequency. Pulse duration at the sample was minimized by using a dispersion compensation system with settings that produced the largest two-photon excited fluorescence for the same laser power. Laser power at the sample was maintained at 3–11 mW with an electrooptic modulator. Laser light was focused on the sample with a 20 × 1.0 N.A. water-immersion Leica objective. Two-photon excited fluorescence was collected by the same lens and, after filtering excitation light by a Chroma ET680sp filter (Chroma Technology Corp.), the beam was directed to either PMT or HyD detectors in a non-descanned manner or to a Leica HyD detector in the descanned configuration. Emission spectra were obtained with TCS SP5 spectrally sensitive HyD detector in a descanned configuration. For imaging the RPE and retina in the intact, enucleated mouse eye, both the laser light and the resulting fluorescence had to penetrate through the sclera. Before eye enucleation, mice were anesthetized by i.p. injection of 20 μL/g body weight of 6 mg/mL ketamine and 0.44 mg/mL xylazine diluted with 10 mM sodium phosphate, pH 7.2, containing 100 mM NaCl and then euthanized in compliance with American Veterinary Medical Association Guidelines on Euthanasia, and approval by the Case Western Reserve University Institutional Animal Care and Use Committee. TPM 3D reconstructions and pixel gray values of raw retinal images were analyzed offline with Leica LAS AF 3.0.0. Sigma Plot 11.0 software (Systat Software, Inc.) was used for statistical analyses.

ERG Recordings. All ERG experimental procedures were performed under dim red light transmitted through a Kodak No. 1 safelight filter (transmittance >560 nm) as previously described (11, 90). Briefly, mice were initially dark-adapted overnight before recording; they were then anesthetized under a safety light by i.p. injection of 20 μL/g body weight of 6 mg/mL ketamine and 0.44 mg/mL xylazine diluted with 10 mM sodium phosphate, pH 7.2, containing 100 mM NaCl. Pupils were dilated with a mixture of 0.5% tropicamide and 0.5% phenylephrine hydrochloride. A contact lens electrode was placed on the eye, and a reference electrode and ground electrode were positioned on the ear and tail, respectively. ERGs were recorded by the universal testing and electrophysiological system with BigShot Ganzfeld (LKC Technologies). Single-flash recording was performed. White-light flash stimuli were used over a range of intensities (from −3.7 to 1.6 log cd·s·m^{-2}), and flash durations were adjusted according to intensity (from 20 μs to 1 ms). Two to five recordings were made at sufficient intervals between flash stimuli (from 3 s to 1 min) to allow mice time to recover.

Retinoid Analyses. Retinoid extraction, derivatization, and separation by HPLC were performed on eye samples from dark-adapted mice as previously described (91, 92). Briefly, eyes were homogenized in 1 mL of retinoid analysis buffer [50 mM Mops, 10 mM NH_2OH, and 50% (vol/vol) ethanol in 50% (vol/vol) H_2O (pH 7.0)]. Retinoids were extracted twice with 4 mL of hexane. Then the extracted retinoids in the organic solvent were dried down in a SpeedVac The retinoids were resuspended in 0.3 mL of hexane and separated by normal-phase HPLC (Ultrasphere-Si, 4.6 μm 3× 250 mm; Beckman Coulter) with 10% ethyl acetate and 90% hexane at a flow rate of 1.4 mL/min.

Scanning Laser Ophthalmoscopy. SLO imaging was done with an HRAII instrument (Heidelberg Engineering). Mice were anesthetized by i.p. injection of a mixture (20 μL/g body weight) containing ketamine (6 mg/mL) and xylazine (0.44 mg/mL) in 10 mM sodium phosphate, pH 7.2, with 100 mM NaCl. Pupils were dilated with a mixture of 0.5% tropicamide and 0.5% phenylephrine hydrochloride before the procedure. The number of AF particles were counted per image.

Histological Analyses. All procedures used for sample preparation, immunohistochemistry, and light microscopy were performed by well-established methods published previously (31). Mouse anti-rhodopsin 1D4 antibody (1:100; a gift from Robert Molday, University of British Columbia, Vancouver) and mouse anti–ZO-1 antibody (Invitrogen) were used for immunostaining. TUNEL staining was carried out with an ApoTag Peroxidase in Situ Apoptosis Detection Kit (Chemicon). Electron microscopic analyses were performed as previously described (11).

Retinal Tissue Cultures. Eyes were enucleated, washed with a penicillin–streptomycin solution (Sigma), and rinsed with Hank's balanced salt solution (HyClone). Prepared mouse eyecups were flattened by creating retinal flaps. Flattened retinas were transferred onto filter paper and the retina was gently peeled off from the RPE/choroid. All these procedures were performed under a surgical microscope. Each retina on filter paper was placed into a well of a 12-well plate filled with 0.5 mL of DMEM (HyClone) with 10% FBS and incubated for 16 h at 37 °C. Retinas then were washed twice with 0.5 mL of fresh DMEM containing 10% FBS and finally incubated again with/without 30 μM of atRAL for 6 h at 37 °C. A lactate dehydrogenase (LDH) assay was performed to determine cellular death rates with a LDH activity assay kit (BioVision). The percentage of cytotoxicity was calculated as [(a retina with atRAL − a retina without atRAL)/(lysis control − a retina without atRAL)] × 100.

MS Analyses of Mouse Retina. At day 3 after light exposure, mouse retinas were dissected and homogenized in 0.3 mL of ice-cold acetonitrile. Samples were vortexed for 30 s followed by centrifugation for 15 min at 16,000 × *g*. Clear supernatants were collected and used directly for LC/MS analyses. Each retinal extract was injected onto a reverse-phase C18 Phenomenex HPLC column (250 × 4.60 mm; 5 μm) preequilibrated with 5% acetonitrile in water. Chemical components of the retina were eluted in a linear gradient of acetonitrile from 5% to 100% (vol/vol) developed within 50 min at flow rate of 0.7 mL/min and directed onto LXQ linear ion trap MS spectrometer (Thermo Scientific) via an electrospray ionization interface operated in the positive ionization mode. Parameters for both chemical ionization and the instrument were optimized for retinal condensation products such as A2E. All solvents contained 0.1% formic acid. Total ion chromatograms were analyzed with XCMS software (45) available online at the Scripps Center for Metabolomics (93).

Statistical Analyses. Data representing the means ± SD for the results of at least three independent experiments were compared by one-way ANOVA with $P < 0.05$ considered statistically significant.

ACKNOWLEDGMENTS. We thank Dr. L. T. Webster, Jr. (Case Western Reserve University) and members of K.P.'s laboratory for helpful comments on this manuscript. We thank Y. Chen, M. Rozanowska, H. Fujioka, and M. Hitomi (Case Western Reserve University) and W. Sun (Polgenix Inc.) for their comments and technical support. This work was supported by funding from the National Eye Institute National Institutes of Health Grants R24EY021126 (to K.P.), R01EY009339 (to K.P.), R01EY022606 (to K.P.), R01EY022658 (to A.M.), K08EY019031 (to A.M.), K08EY019880 (to T.M.), and P30EY011373; National Institute on Aging, National Institutes of Health Grant R44AG043645 (to G.P.); Research to Prevent Blindness Foundation; the Foundation Fighting Blindness; and the Ohio Lions Eye Research Foundation. K.P. is John H. Hord Professor of Pharmacology.

1. Holz FG, et al.; FAM-Study Group (2007) Progression of geographic atrophy and impact of fundus autofluorescence patterns in age-related macular degeneration. *Am J Ophthalmol* 143(3):463–472.
2. Jacobson SG, et al. (2007) Human cone photoreceptor dependence on RPE65 isomerase. *Proc Natl Acad Sci USA* 104(38):15123–15128.
3. Swanson EA, et al. (1993) In vivo retinal imaging by optical coherence tomography. *Opt Lett* 18(21):1864–1866.
4. Maguire AM, et al. (2008) Safety and efficacy of gene transfer for Leber's congenital amaurosis. *N Engl J Med* 358(21):2240–2248.
5. Bainbridge JW, et al. (2008) Effect of gene therapy on visual function in Leber's congenital amaurosis. *N Engl J Med* 358(21):2231–2239.
6. Cideciyan AV, et al. (2008) Human gene therapy for RPE65 isomerase deficiency activates the retinoid cycle of vision but with slow rod kinetics. *Proc Natl Acad Sci USA* 105(39):15112–15117.
7. Rosenfeld PJ, et al.; MARINA Study Group (2006) Ranibizumab for neovascular age-related macular degeneration. *N Engl J Med* 355(14):1419–1431.
8. Gillies MC, Wong TY (2007) Ranibizumab for neovascular age-related macular degeneration. *N Engl J Med* 356(7):748–749, author reply 749–750.
9. Strauss O (2005) The retinal pigment epithelium in visual function. *Physiol Rev* 85(3): 845–881.
10. Kevany BM, Palczewski K (2010) Phagocytosis of retinal rod and cone photoreceptors. *Physiology (Bethesda)* 25(1):8–15.
11. Maeda A, et al. (2005) Role of photoreceptor-specific retinol dehydrogenase in the retinoid cycle in vivo. *J Biol Chem* 280(19):18822–18832.
12. Maeda A, et al. (2012) Primary amines protect against retinal degeneration in mouse models of retinopathies. *Nat Chem Biol* 8(2):170–178.
13. Kiser PD, Golczak M, Maeda A, Palczewski K (2012) Key enzymes of the retinoid (visual) cycle in vertebrate retina. *Biochim Biophys Acta* 1821(1):137–151.
14. Tsybovsky Y, Orban T, Molday RS, Taylor D, Palczewski K (2013) Molecular organization and ATP-induced conformational changes of ABCA4, the photoreceptor-specific ABC transporter. *Structure* 21(5):854–860.
15. Tsybovsky Y, Molday RS, Palczewski K (2010) The ATP-binding cassette transporter ABCA4: Structural and functional properties and role in retinal disease. *Adv Exp Med Biol* 703:105–125.
16. Tang PH, Kono M, Koutalos Y, Ablonczy Z, Crouch RK (2013) New insights into retinoid metabolism and cycling within the retina. *Prog Retin Eye Res* 32:48–63.
17. von Lintig J, Kiser PD, Golczak M, Palczewski K (2010) The biochemical and structural basis for *trans*-to-*cis* isomerization of retinoids in the chemistry of vision. *Trends Biochem Sci* 35(7):400–410.
18. Maeda A, et al. (2009) Involvement of *all-trans*-retinal in acute light-induced retinopathy of mice. *J Biol Chem* 284(22):15173–15183.
19. Quazi F, Lenevich S, Molday RS (2012) ABCA4 is an N-retinylidene-phosphatidylethanolamine and phosphatidylethanolamine importer. *Nat Commun* 3:925.
20. Rattner A, Smallwood PM, Nathans J (2000) Identification and characterization of *all-trans*-retinol dehydrogenase from photoreceptor outer segments, the visual cycle enzyme that reduces all-trans-retinal to all-trans-retinol. *J Biol Chem* 275(15):11034–11043.
21. Allikmets R, et al. (1997) A photoreceptor cell-specific ATP-binding transporter gene (ABCR) is mutated in recessive Stargardt macular dystrophy. *Nat Genet* 15(3):236–246.
22. Allikmets R, et al. (1997) Mutation of the Stargardt disease gene (ABCR) in age-related macular degeneration. *Science* 277(5333):1805–1807.
23. Sparrow JR, et al. (2012) The bisretinoids of retinal pigment epithelium. *Prog Retin Eye Res* 31(2):121–135.
24. Parish CA, Hashimoto M, Nakanishi K, Dillon J, Sparrow J (1998) Isolation and one-step preparation of A2E and iso-A2E, fluorophores from human retinal pigment epithelium. *Proc Natl Acad Sci USA* 95(25):14609–14613.
25. Mata NL, Weng J, Travis GH (2000) Biosynthesis of a major lipofuscin fluorophore in mice and humans with ABCR-mediated retinal and macular degeneration. *Proc Natl Acad Sci USA* 97(13):7154–7159.
26. Eldred GE, Lasky MR (1993) Retinal age pigments generated by self-assembling lysosomotropic detergents. *Nature* 361(6414):724–726.
27. Holz FG, Bellman C, Staudt S, Schütt F, Völcker HE (2001) Fundus autofluorescence and development of geographic atrophy in age-related macular degeneration. *Invest Ophthalmol Vis Sci* 42(5):1051–1056.
28. Fleckenstein M, et al. (2009) Discrete arcs of increased fundus autofluorescence in retinal dystrophies and functional correlate on microperimetry. *Eye (Lond)* 23(3): 567–575.
29. Maeda A, Maeda T, Golczak M, Palczewski K (2008) Retinopathy in mice induced by disrupted all-trans-retinal clearance. *J Biol Chem* 283(39):26684–26693.
30. Golczak M, Kuksa V, Maeda T, Moise AR, Palczewski K (2005) Positively charged retinoids are potent and selective inhibitors of the *trans-cis* isomerization in the retinoid (visual) cycle. *Proc Natl Acad Sci USA* 102(23):8162–8167.
31. Chen Y, et al. (2012) Mechanism of all-trans-retinal toxicity with implications for stargardt disease and age-related macular degeneration. *J Biol Chem* 287(7):5059–5069.
32. Palczewska G, et al. (2010) Noninvasive multiphoton fluorescence microscopy resolves retinol and retinal condensation products in mouse eyes. *Nat Med* 16(12):1444–1449.
33. Imanishi Y, Batten ML, Piston DW, Baehr W, Palczewski K (2004) Noninvasive two-photon imaging reveals retinyl ester storage structures in the eye. *J Cell Biol* 164(3): 373–383.
34. Golczak M, et al. (2005) Lecithin:retinol acyltransferase is responsible for amidation of retinylamine, a potent inhibitor of the retinoid cycle. *J Biol Chem* 280(51):42263–42273.
35. Imanishi Y, Sun W, Maeda T, Maeda A, Palczewski K (2008) Retinyl ester homeostasis in the adipose differentiation-related protein-deficient retina. *J Biol Chem* 283(36): 25091–25102.
36. Hunter JJ, et al. (2010) Images of photoreceptors in living primate eyes using adaptive optics two-photon ophthalmoscopy. *Biomed Opt Express* 2(1):139–148.
37. Imanishi Y, Palczewski K (2010) Visualization of retinoid storage and trafficking by two-photon microscopy. *Methods Mol Biol* 652:247–261.
38. Orban T, Palczewska G, Palczewski K (2011) Retinyl ester storage particles (retinosomes) from the retinal pigmented epithelium resemble lipid droplets in other tissues. *J Biol Chem* 286(19):17248–17258.
39. Okano K, et al. (2012) Retinal cone and rod photoreceptor cells exhibit differential susceptibility to light-induced damage. *J Neurochem* 121(1):146–156.
40. Joly S, et al. (2009) Cooperative phagocytes: Resident microglia and bone marrow immigrants remove dead photoreceptors in retinal lesions. *Am J Pathol* 174(6): 2310–2323.
41. Luhmann UF, et al. (2009) The drusenlike phenotype in aging Ccl2-knockout mice is caused by an accelerated accumulation of swollen autofluorescent subretinal macrophages. *Invest Ophthalmol Vis Sci* 50(12):5934–5943.
42. Kohno H, et al. (2013) Photoreceptor proteins initiate microglial activation via Toll-like receptor 4 in retinal degeneration mediated by all-trans-retinal. *J Biol Chem* 288(21): 15326–15341.
43. Xu H, Chen M, Forrester JV (2009) Para-inflammation in the aging retina. *Prog Retin Eye Res* 28(5):348–368.
44. Jung S, et al. (2000) Analysis of fractalkine receptor CX(3)CR1 function by targeted deletion and green fluorescent protein reporter gene insertion. *Mol Cell Biol* 20(11): 4106–4114.
45. Benton HP, Wong DM, Trauger SA, Siuzdak G (2008) XCMS2: Processing tandem mass spectrometry data for metabolite identification and structural characterization. *Anal Chem* 80(16):6382–6389.
46. Batten ML, et al. (2004) Lecithin-retinol acyltransferase is essential for accumulation of all-trans-retinyl esters in the eye and in the liver. *J Biol Chem* 279(11):10422–10432.
47. Komeima K, Usui S, Shen J, Rogers BS, Campochiaro PA (2008) Blockade of neuronal nitric oxide synthase reduces cone cell death in a model of retinitis pigmentosa. *Free Radic Biol Med* 45(6):905–912.
48. Stefanska J, Pawliczak R (2008) Apocynin: Molecular aptitudes. *Mediators Inflamm* 2008:106507.
49. Simons JM, Hart BA, Ip Vai Ching TR, Van Dijk H, Labadie RP (1990) Metabolic activation of natural phenols into selective oxidative burst agonists by activated human neutrophils. *Free Radic Biol Med* 8(3):251–258.
50. Willott E, et al. (1993) The tight junction protein ZO-1 is homologous to the Drosophila discs-large tumor suppressor protein of septate junctions. *Proc Natl Acad Sci USA* 90(16):7834–7838.
51. Boulton M, Dayhaw-Barker P (2001) The role of the retinal pigment epithelium: Topographical variation and ageing changes. *Eye (Lond)* 15(Pt 3):384–389.
52. Duncan JL, et al. (2003) An RCS-like retinal dystrophy phenotype in mer knockout mice. *Invest Ophthalmol Vis Sci* 44(2):826–838.
53. Gal A, et al. (2000) Mutations in MERTK, the human orthologue of the RCS rat retinal dystrophy gene, cause retinitis pigmentosa. *Nat Genet* 26(3):270–271.
54. Vollrath D, et al. (2001) Correction of the retinal dystrophy phenotype of the RCS rat by viral gene transfer of Mertk. *Proc Natl Acad Sci USA* 98(22):12584–12589.
55. Radu RA, et al. (2011) Complement system dysregulation and inflammation in the retinal pigment epithelium of a mouse model for Stargardt macular degeneration. *J Biol Chem* 286(21):18593–18601.
56. Hughes EH, et al. (2003) Generation of activated sialoadhesin-positive microglia during retinal degeneration. *Invest Ophthalmol Vis Sci* 44(5):2229–2234.
57. Gupta N, Brown KE, Milam AH (2003) Activated microglia in human retinitis pigmentosa, late-onset retinal degeneration, and age-related macular degeneration. *Exp Eye Res* 76(4):463–471.
58. Ding X, Patel M, Chan CC (2009) Molecular pathology of age-related macular degeneration. *Prog Retin Eye Res* 28(1):1–18.
59. Ma W, Zhao L, Fontainhas AM, Fariss RN, Wong WT (2009) Microglia in the mouse retina alter the structure and function of retinal pigmented epithelial cells: A potential cellular interaction relevant to AMD. *PLoS ONE* 4(11):e7945.
60. McBee JK, Palczewski K, Baehr W, Pepperberg DR (2001) Confronting complexity: the interlink of phototransduction and retinoid metabolism in the vertebrate retina. *Prog Retin Eye Res* 20(4):469–529.

61. Kiser PD, Golczak M, Palczewski K (2014) Chemistry of the retinoid (visual) cycle. *Chem Rev* 114(1):194–232.
62. Palczewski K, Orban T (2013) From atomic structures to neuronal functions of G protein-coupled receptors. *Annu Rev Neurosci* 36:139–164.
63. Palczewski K (2006) G protein-coupled receptor rhodopsin. *Annu Rev Biochem* 75:743–767.
64. Sparrow JR (2010) Bisretinoids of RPE lipofuscin: Trigger for complement activation in age-related macular degeneration. *Adv Exp Med Biol* 703:63–74.
65. Hunter JJ, et al. (2012) The susceptibility of the retina to photochemical damage from visible light. *Prog Retin Eye Res* 31(1):28–42.
66. Amengual J, et al. (2011) A mitochondrial enzyme degrades carotenoids and protects against oxidative stress. *FASEB J* 25(3):948–959.
67. Lobo GP, Isken A, Hoff S, Babino D, von Lintig J (2012) BCDO2 acts as a carotenoid scavenger and gatekeeper for the mitochondrial apoptotic pathway. *Development* 139(16):2966–2977.
68. Siems W, et al. (2002) Beta-carotene cleavage products induce oxidative stress in vitro by impairing mitochondrial respiration. *FASEB J* 16(10):1289–1291.
69. Cuperus R, Leen R, Tytgat GA, Caron HN, van Kuilenburg AB (2010) Fenretinide induces mitochondrial ROS and inhibits the mitochondrial respiratory chain in neuroblastoma. *Cell Mol Life Sci* 67(5):807–816.
70. Williams TP, Squitieri A, Henderson RP, Webbers JP (1999) Reciprocity between light intensity and rhodopsin concentration across the rat retina. *J Physiol* 516(Pt 3): 869–874.
71. Williams TP, Webbers JP, Giordano L, Henderson RP (1998) Distribution of photon absorption rates across the rat retina. *J Physiol* 508(Pt 2):515–522.
72. Williams TP, Henrich S, Reiser M (1998) Effect of eye closures and openings on photostasis in albino rats. *Invest Ophthalmol Vis Sci* 39(3):603–609.
73. Penn JS, Williams TP (1986) Photostasis: Regulation of daily photon-catch by rat retinas in response to various cyclic illuminances. *Exp Eye Res* 43(6):915–928.
74. Marc RE, et al. (2008) Extreme retinal remodeling triggered by light damage: Implications for age related macular degeneration. *Mol Vis* 14:782–806.
75. Liang Y, et al. (2004) Rhodopsin signaling and organization in heterozygote rhodopsin knockout mice. *J Biol Chem* 279(46):48189–48196.
76. Humphries MM, et al. (1997) Retinopathy induced in mice by targeted disruption of the rhodopsin gene. *Nat Genet* 15(2):216–219.
77. Lem J, et al. (1999) Morphological, physiological, and biochemical changes in rhodopsin knockout mice. *Proc Natl Acad Sci USA* 96(2):736–741.
78. Wen XH, et al. (2009) Overexpression of rhodopsin alters the structure and photoresponse of rod photoreceptors. *Biophys J* 96(3):939–950.
79. Fletcher EL (2010) Mechanisms of photoreceptor death during retinal degeneration. *Optom Vis Sci* 87(4):269–275.
80. Nicholls DG (2009) Spare respiratory capacity, oxidative stress and excitotoxicity. *Biochem Soc Trans* 37(Pt 6):1385–1388.
81. Yadava N, Nicholls DG (2007) Spare respiratory capacity rather than oxidative stress regulates glutamate excitotoxicity after partial respiratory inhibition of mitochondrial complex I with rotenone. *J Neurosci* 27(27):7310–7317.
82. Chertov AO, et al. (2011) Roles of glucose in photoreceptor survival. *J Biol Chem* 286(40):34700–34711.
83. Cornwall MC, Fein A, MacNichol EF, Jr. (1990) Cellular mechanisms that underlie bleaching and background adaptation. *J Gen Physiol* 96(2):345–372.
84. Sparrow JR, Hicks D, Barnstable CJ (1990) Cell commitment and differentiation in explants of embryonic rat neural retina. Comparison with the developmental potential of dissociated retina. *Brain Res Dev Brain Res* 51(1):69–84.
85. Pinzón-Duarte G, Kohler K, Arango-González B, Guenther E (2000) Cell differentiation, synaptogenesis, and influence of the retinal pigment epithelium in a rat neonatal organotypic retina culture. *Vision Res* 40(25):3455–3465.
86. Yanagi Y, Inoue Y, Jang WD, Kadonosono K (2006) A2e mediated phototoxic effects of endoilluminators. *Br J Ophthalmol* 90(2):229–232.
87. Sparrow JR, Parish CA, Hashimoto M, Nakanishi K (1999) A2E, a lipofuscin fluorophore, in human retinal pigmented epithelial cells in culture. *Invest Ophthalmol Vis Sci* 40(12):2988–2995.
88. Zhou J, Jang YP, Kim SR, Sparrow JR (2006) Complement activation by photooxidation products of A2E, a lipofuscin constituent of the retinal pigment epithelium. *Proc Natl Acad Sci USA* 103(44):16182–16187.
89. Batten ML, et al. (2005) Pharmacological and rAAV gene therapy rescue of visual functions in a blind mouse model of Leber congenital amaurosis. *PLoS Med* 2(11):e333.
90. Maeda T, Lem J, Palczewski K, Haeseleer F (2005) A critical role of CaBP4 in the cone synapse. *Invest Ophthalmol Vis Sci* 46(11):4320–4327.
91. Van Hooser JP, et al. (2002) Recovery of visual functions in a mouse model of Leber congenital amaurosis. *J Biol Chem* 277(21):19173–19182.
92. Van Hooser JP, et al. (2000) Rapid restoration of visual pigment and function with oral retinoid in a mouse model of childhood blindness. *Proc Natl Acad Sci USA* 97(15): 8623–8628.
93. Tautenhahn R, Patti GJ, Rinehart D, Siuzdak G (2012) XCMS Online: A web-based platform to process untargeted metabolomic data. *Anal Chem* 84(11):5035–5039.